e-ISSN 2320 –7876 www.ijfans.org

Research Paper

Vol.11, Iss.9, Dec 2022

MULTI WAVELENGTH ANALYSIS OF SOLAR ERUPTION SOURCE REGIONS

SATHIYA. M
Research Scholar
M.Phil Physics
Bharath Institute Of Higher Education And Research
Mail Id : mssathiya19@gmail.com

Dr.K.THIYAGARAJAN
Head of the Department, Department Of Physics
Bharath Institute Of Higher Education And Research
Address for Correspondence

SATHIYA. M
Research Scholar
M.Phil Physics
Bharath Institute Of Higher Education And Research
Mail Id : mssathiya19@gmail.com

Abstract

At the outset, we briefly introduce the physical phenomena and salient features of structure of the Sun. We elaborate the eruptions and emissions that occur on the Sun. On the basis of spectra and the temperature the Sun is classified as a *G2V* star. The proximity of the Earth with the Sun facilitates a detailed study of the surface of the Sun, atmosphere and activities which are similar in most stars. This study also provides an important opportunity on various dynamical physical processes in explicit spatial and temporal resolutions for the stars of similar masses and similar stages of evolution. There are many interesting, strange changes which take place in the interior and the atmosphere of the Sun. The Sun has a strong, complex magnetic field which can infuse the solar atmosphere with sunspots and powerful explosive events such as flares, prominence eruptions and ejection of massive particles. The Sun is a prominent star and the centre of our solar system. On the basis of spectra of solar radiations and the temperature, the Sun is classified as a *G2V* star. The Sun is the primary source of light and energy for life on Earth. Thus, it is all the more important to understand the physical and astronomical nature of the universe. The Sun 4.6

Research Paper

Vol.11, Iss.9, Dec 2022

billion years old and is expected to live further 4.6 billion years. It has a mass of 1.99×10^{30} kg and radius of the order 6.95×10^{8}m . The distance between the Earth and the Sun is ~ 1.49×10^{11}m that is known as One Astronomical Unit (1 *AU*) . The surface temperature of the Sun is about ~ 5800°C .

INTRODUCTION

The Sun has luminosity of the order of 3.84×10^{26}w. The chemical composition on its surface, in terms of mass, is as follows: Hydrogen (71%), Helium (27%) and other metals (2%) of which the most abundant are Oxygen, Carbon, Iron, Neon and Nitrogen respectively (Phillips, 1992). The Sun is believed to be a middle aged star through its life with an expected age of ~ 4.6×10^{9}years. The prominent activities on the Sun are sunspots, powerful explosive events such as flares, prominences, eruptions and coronal mass ejections (CMEs).

Structure of the Sun

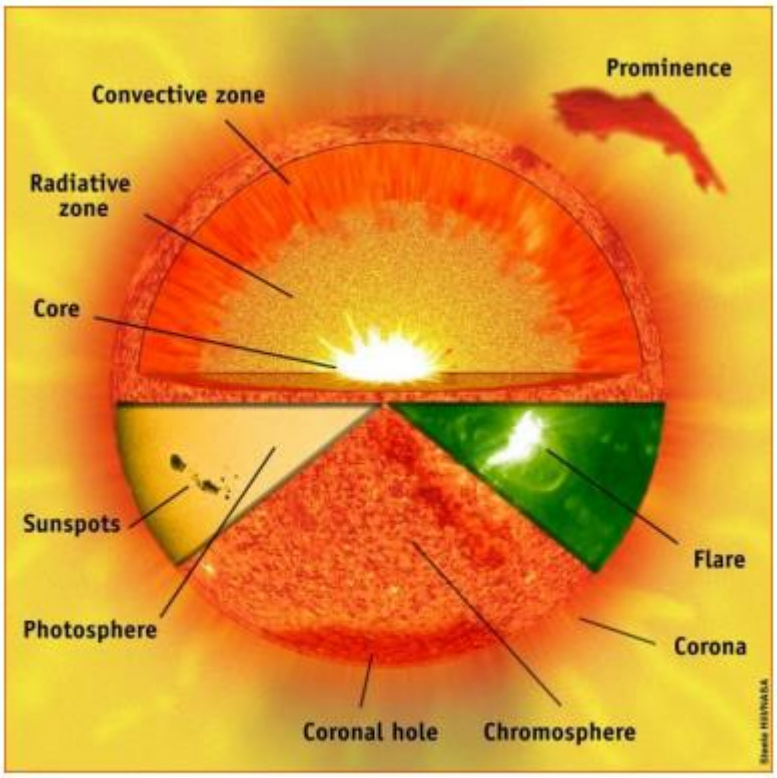

Fig. 1.1: The structure of the Sun and solar activity features: Schematic Cross-section (Courtesy SOHO/NASA)

e-ISSN 2320 –7876 www.ijfans.org
Research Paper
Vol.11, Iss.9, Dec 2022

The Sun has different layers that form its structure, but, it is difficult to get any direct observational evidence relevant to the internal structure. The understanding of the interior of the Sun is based on rigorous theoretical calculations and on assumptions based on the Sun's composition, the mass, the radius, the state of gas and the temperature and the energy source. During the recent past, a new powerful technique has emerged that can probe the solar interior of the Sun, is known as helioseismology (Howe, 2009). In recent times astronomical observations have significantly improved about the understanding of the physical state and physical properties of the Sun.

The Chromosphere and Transition region

The chromosphere is a thin layer of the solar atmosphere just above the photosphere. From the top of the photosphere temperature trends upwards from K oo 4500° to 1000 ° k in the chromospheres and the density of gases drops gradually. It can only be observed as a thin red band at the edge of the Sun during a solar eclipse. It appears reddish in color because of strong $H_\alpha$emission (6563 $^{)o}$ A . At the top of the chromospheres, towards the corona the uppermost layer of the Sun, the temperature increases to up to 10 ^{6} K. The chromospheres exhibits a number of features such as plages, spicules, filament/prominences. and are describebelow. Plages are the bright patches surrounding sunspots that are best seen in H_α . The spicules are spike–like structures that extend from the solar chromospheres up to the corona. These are short–lived phenomena that last only a few minutes.

The Corona

The outer atmosphere of the Sun is called corona. Temperature of the corona is ~ 2×10^6K, but, its density is much less than the temperature of the chromospheres. It can only be observed during Total Solar Eclipse or through a coronagraph. The coronal loops are the magnetic field loops that pass through the corona and join regions of opposite magnetic polarity in the underlying photosphere. Coronal loops are expected to have exceptionally strong magnetic fields, and they contain dense hot coronal gases (at about million–degree or more temperature) that emit intense X–ray radiations. Coronal holes are the darker and the least active regions in the corona of the Sun (Cranmer, 2009). The density and temperature in the coronal holes are lower than the temperature in the other parts of the corona. These are the regions of open magnetic field that do not immediately return back to the Sun and from where high–speed solar winds stream out. The low

Research Paper

Vol.11, Iss.9, Dec 2022

density of the gas makes these parts of thecorona appear dark in Extreme Ultra-Violet (EUV) and soft X–ray images of the Sun. They generally appear near the polar region of the Sun.

SOLAR ERUPTIVE PHENOMENA

The first recorded observation of a solar flare was made by R. C. Carrington in 1859 at his private observatory at Redhill, outside London. Carrington (1859) was engaged in his daily sunspot drawing in the forenoon on 1 September 1859 when he first noticed the flare. The white-light emission was initially visible at points A and B and during the courses of five minutes moved about 50000 km to points C and D where it vanished as two rapidly fading dots of white light. Carrington expressed surprise that the conflagration had in no way alerted the appearance of the sunspot group which he had finished drawing before the occurrence. Fortunately, Carringtons observation was confirmed by Hodgson (1859), an amateur astronomer who was observing nearby

.

The history of flare research can be divided into three main periods (for a detailed review see Svestka et al. 1992). The first period from 1859-1934 spans the careers of Carrington and Hale. This period is notable for the relative lack

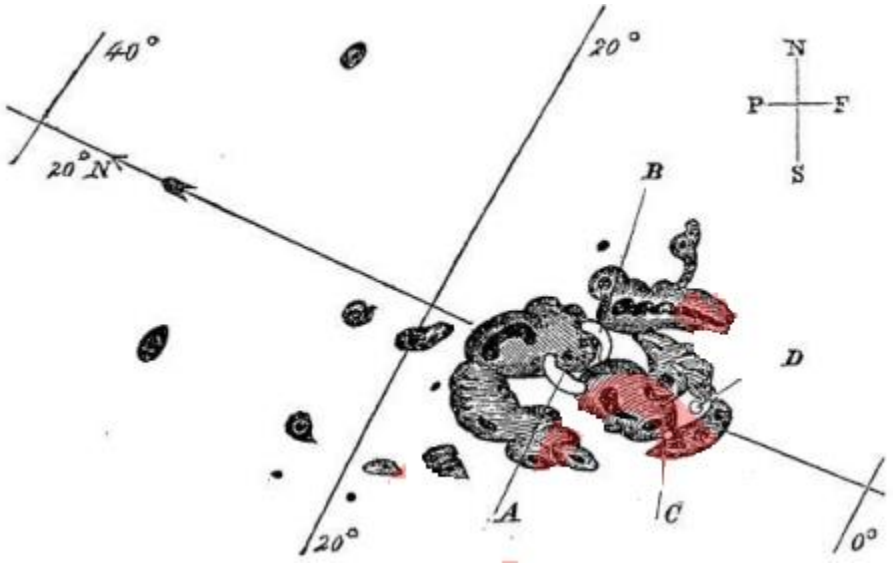

Figure 2.1 Sketch of the first reported solar flare.

The flare was observed by Carrington in white light on 1859 September 1 (Carrington, 1859). White regions marked as A, B, C, and D are the flaring regions

of progress. The published record of major flares for this 75 year interval encompasses only about 35 events, consisting of fortuitous observations of white-light flares, reports by early spectroscopists of reversals of line emission near sunspots, and, after 1892, flares observed with the Hale spectroheliograph. With this spectroheliograph, Hale obtained the first published photographs of a solar flare on 15 July 1892 (Svestka et al. 1992). The spectrohelioscope (an instrument that allowed the entire Sun to be scanned visually at selected wavelengths) developed by Hale during the 1920s was responsible for the rapid advance in the knowledge of flares that took place in the next era of flare research from 1935-1963. The institution of a world-wide flare patrol brought significant advances in knowledge of flares in the 1930s an 1940s and new window were opened to observe flares at short (soft X-ray, which was indicated by the sudden ionospheric disturbances; Kreplin et al. 1962) and long (radio) wavelengths. In the 1950s and 1960s metric radio bursts were related to trapped energetic electrons and shocks, and two-ribbon flares were associated with energetic protons in space .

Radio and X-ray observations gave evidence for two basic types of flare processes: an impulsive phased followed by a long-duration or gradual phase. Itwas found that flares were often preceded by filament activations, and growing loop prominence systems were recognized as the limb counterpart of two-ribbon disk flares. This middle era of flare research has a data survey and classification character that is well-captured by the book Solar Flares by Smith & Smith (1963).

The modern era, since 1963, is characterized by space observations and a trend toward synthesis indicated by the development of increasingly sophisticated and comprehensive models of the flare phenomena. The early 1970s brought Skylab observations of coronal mass ejections (CMEs) and arcades of coronal soft X-ray loops above two-ribbon flares. In the mid-1970s, the Kopp-Penuman reconnection model, based on configurations proposed earlier by Carmichael, Sturrock, and Hirayama, provided a framework in which the newly discovered CMEs could be related to the basic characteristic of two-ribbon flares. The 1980s brought key new results from SMM and Hinotori including images of hard X-ray flares and large-scale coronal structures associated with eruptive flares. The key new results from Yohkoh in the 1990s are: evidence for on-going magnetic reconnection in solar flares, i.e., cusp-shaped soft X-ray arcades in long-duration flares and above-the-loop-top hard X-ray sources in impulsive flares; sigmoidal soft X-ray structures in active regions identified as signatures of the likely onset of flares and CMEs;

arcade formation and coronal dimming identified as the soft X-ray counter part of a CMEs (Kosugi& Acton, 2002). In the 2000s, RHESSI (Lin et al., 2002) has provided the first capability for gamma-ray imaging as well as high-resolution spectroscopy of ion-produced gamma-ray lines and X-ray imaging spectroscopy of the bremstrahlung radiation from energetic electrons. One of the key new results of RHESSI is gamma-ray line imaging of solar flares implies spatial differences in acceleration and/or propagation between the flare-accelerated ions and electron (Hurford et al., 2006, 2003).

MULTI-WAVE LENGTH VIEW OF SOLAR ACTIVE REGION

The solar and heliospheric activities reported in this paper correspond to the major eruptive activities for three periods. In above mentioned these particular most active durations, first period (22-29 Oct 2013) for active region NOAA AR -11875, AR-11877, AR-11882 and second period (01-08 Nov 2013) for AR NOAA-11882; NOAA AR-11884 and AR-11890; third period (25Oct-08Nov 2014) for NOAA AR-12192, AR-12201 and AR-12205; forth active period 07-15 Mar 2015) for NOAA AR- and fifth active region (02-10 Sep 2017) are the active regions whose transmitting from mean location of heliographic solar disk. To compare the photospheric structure of the active regions with the overlying chromospheric and coronal layers, we show HMI magnetogram and AIA 94 Å images of the active regions in panel (a) (b) and (c) for all three selected active periods respectively. From these HMI magnetogram and AIA 94 Å images we can see the heliospheric position of selected active regions for most active period. The HMI magnetograms, showing the distribution of sunspot and their magnetic polarity. White and black color in HMI magnetogram indicate the positive and negative magnetic polarity region respectively, in the photosphere.

Further we image the reported active regions with SDO AIA 94 Å (in the first coloumn) and HMI magnetograms (in the second coloumn) when the active region passes through central meridian of solar disk. It is well known that when the active region passes through ±45 degree from the centre of solar disk, during that the eruptive CMEs would be Halos and those halo CME will may be produce geomagnetic disturbances.

e-ISSN 2320 –7876 www.ijfans.org

Research Paper

Vol.11, Iss.9, Dec 2022

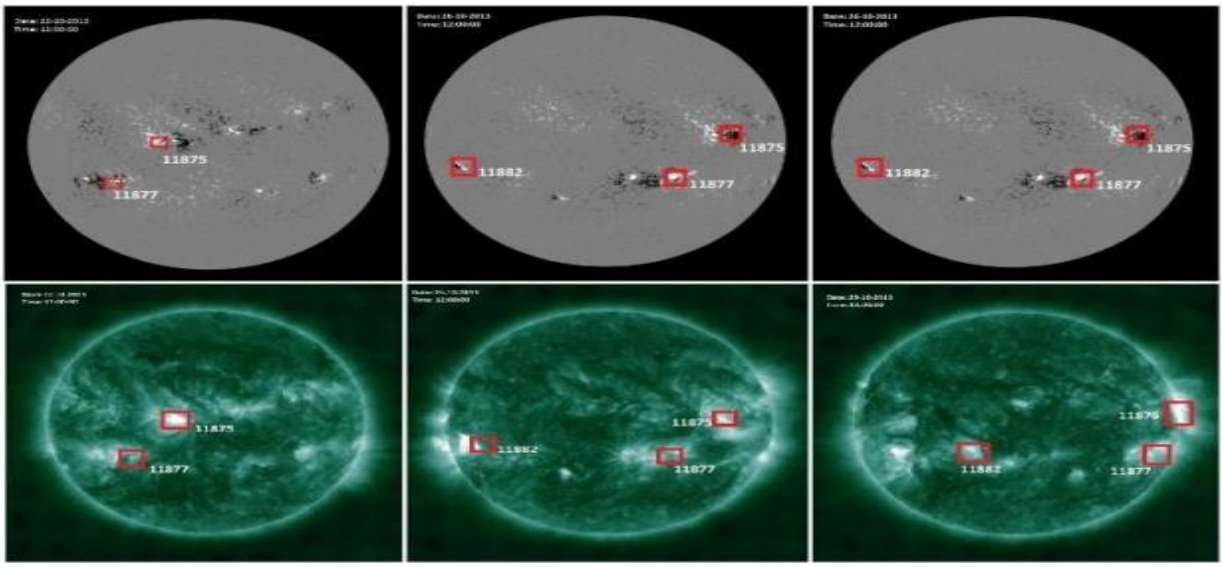

Figure 3.1: Multi-wavelength view of Active regions showing the location where sunspot occurred during active period 22-29 Oct 2013. The above row of images are the HMI magnetograms, showing the distribution of sunspot and their magnetic polarity. White and black colour in HMI magneto gram indicate the positive and negative magnetic polarity region respectively, in the photosphere. In above image, the below row of image are AIA 94 image of active regions showing hot coronal loops of AR NOAA 11875, 11877 and 11882.

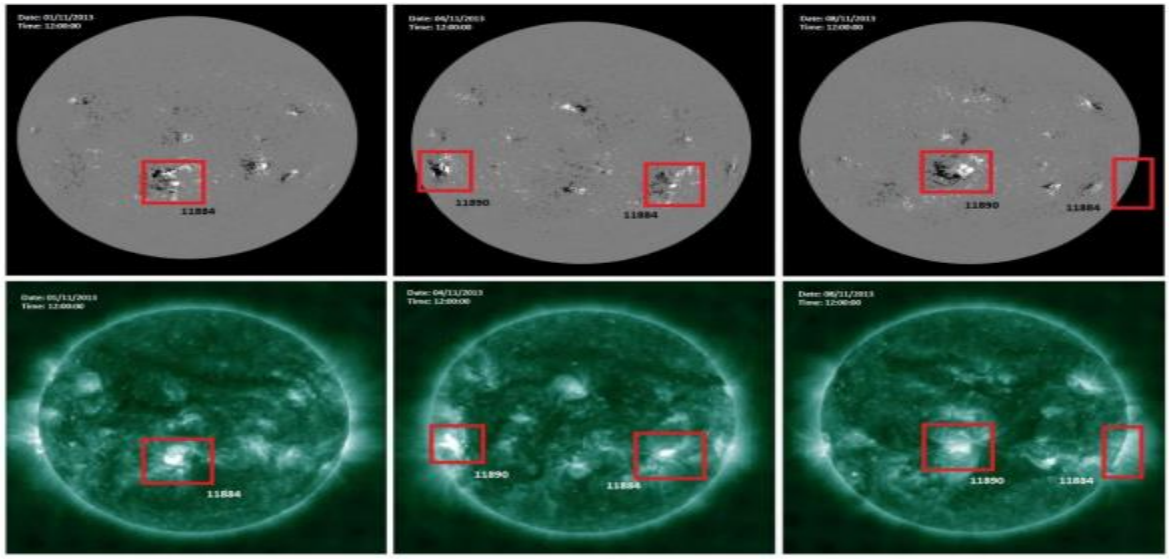

Figure 3.2: Multi-wavelength view of Active regions showing the location where sunspot occurred during active period 01-08 Nov 2013. The above row of images are the HMI magnetograms, showing the distribution of sunspot and their magnetic polarity. White and black

e-ISSN 2320 –7876 www.ijfans.org

Research Paper

Vol.11, Iss.9, Dec 2022

colour in HMI magneto gram indicate the positive and negative magnetic polarity region respectively, in the photosphere. In above image, the below row of image are AIA 94 image of active regions showing hot coronal loops of AR NOAA 11884 and 11890.

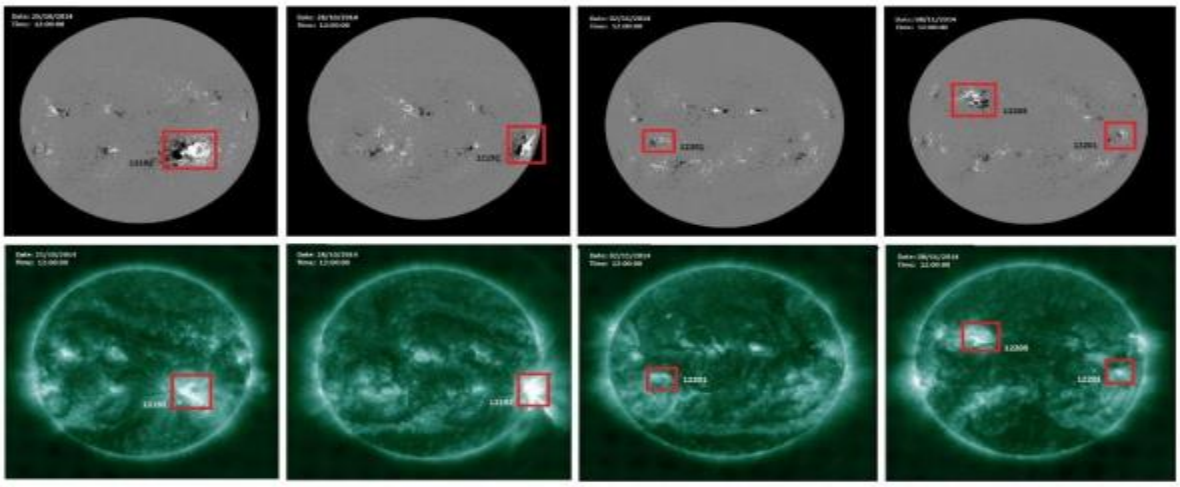

Figure 3.3: Multi-wavelength view of Active regions showing the location where sunspot occurred during selected active period 25 Oct- 08-Nov 2014. In all three panels, the above row of images are the HMI magnetograms, showing the distribution of sunspot and their magnetic polarity. White and black color in HMI magneto gram indicate the positive and negative magnetic polarity region respectively, in the photosphere. In panels, the below row of images are AIA 94 image of active regions showing hot coronal loops for active regions AR NOAA 12192, 12201 and 12205.

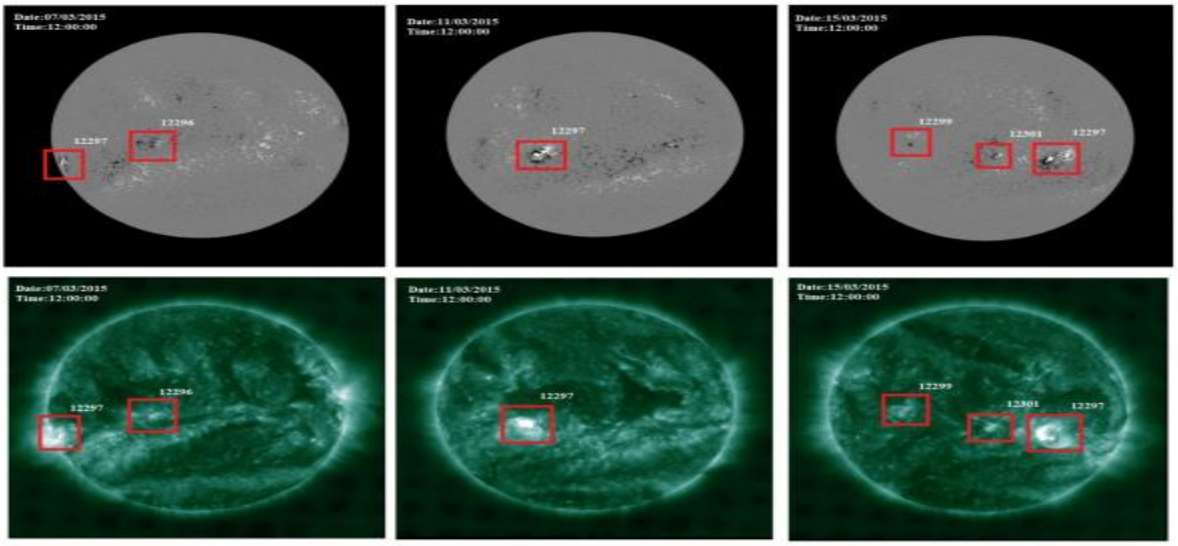

e-ISSN 2320 –7876 www.ijfans.org

Research Paper

Vol.11, Iss.9, Dec 2022

Figure 3.4: Multi-wavelength view of Active regions showing the location where sunspot occurred during selected active period 07-15 March 2015. In all three panels, the above row of images are the HMI magnetograms, showing the distribution of sunspot and their magnetic polarity. White and black color in HMI magneto gram indicate the positive and negative magnetic polarity region respectively, in the photosphere. In panels, the below row of images are AIA 94 image of active regions showing hot coronal loops for AR NOAA 12297, 12296, 12299 and 12301.

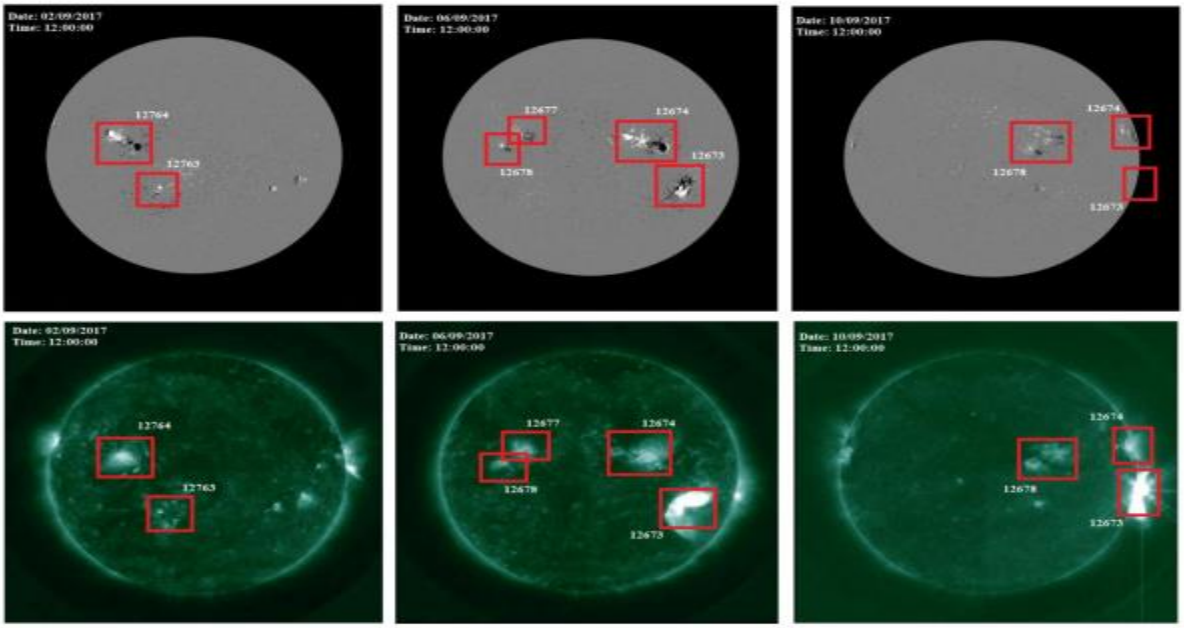

Figure 3.5: Multi-wavelength view of Active regions showing the location where sunspot occurred during selected active period 02-10 sep 2017. In all three panels, the above row of images are the HMI magnetograms, showing the distribution of sunspot and their magnetic polarity. White and black color in HMI magneto gram indicate the positive and negative magnetic polarity region respectively, in the photosphere. In panels, the below row of images are AIA 94 image of active regions showing hot coronal loops for AR NOAA 12673, 12674, 12677, 12678.

Figure 3.6: These solar disks shows the selected active region passes through central meridian of heliospheric disk. In first column we have shown solar disk in AIA 94 Å band and in second column in figure we choose HMI continuum images of solar disk for first active period 22-29 Oct 2013 with three most active region AR 11875, AR 11877 and AR 11882 dated 23/10/2013, 24/10/2013 and 30/10/2013 respectively.

e-ISSN 2320 –7876 www.ijfans.org

Research Paper

Vol.11, Iss.9, Dec 2022

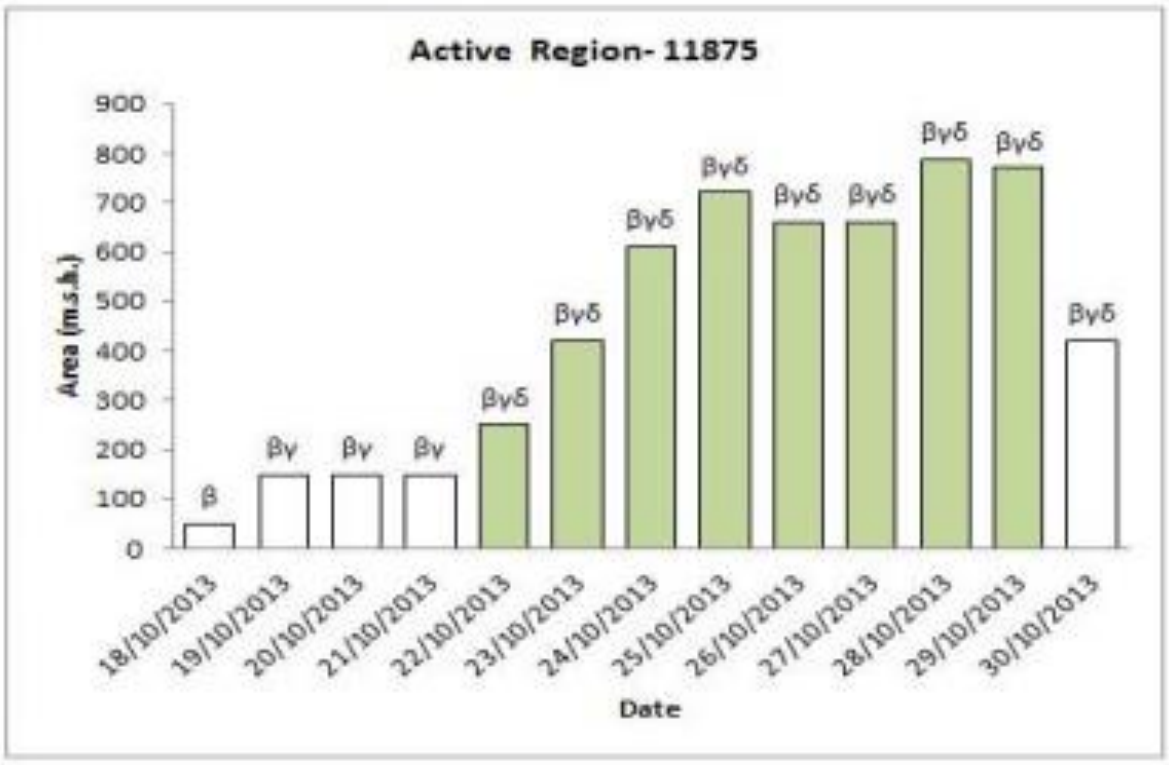

Figure 3.8: Above bar plot shows the growth of Active regions (NOAA 11875, 11882 and 11877) observed during first reported duration 22-29 Oct 2013 in terms of area with respect to days . the shaded green bars shows the days when active region passes through ±45 degree west to east of solar disk.

Table: Show the description of Active region NOAA 11882, the first column shows date, second column indicate the location of region, third column shows area of active region, fourth column shows the magnetic configuration type and last column indicate the flare event occurred from particular active region on particular date.

e-ISSN 2320 –7876 www.ijfans.org

Research Paper

Vol.11, Iss.9, Dec 2022

Active Region- 11877				
	Location	Area	Magnetic Type	Flare events
19-10-2013	S11E75	120	Alpha	
20-10-2013	S12E61	260	Beta	
21-10-2013	S13E55	390	Beta-Gamma	
22-10-2013	S13E38	400	Beta	
23-10-2013	S13E23	390	Beta	C1.3(09:48)
24-10-2013	S12E09	320	Beta-Gamma-Delta	C2.2(17:59), C2.4(14:01), C2.1(04:12), M9.3(00:21)
25-10-2013	S12W03	440	Beta-Gamma	
26-10-2013	S12W16	390	Beta-Gamma	C7.7(18:50), C2.8(13:19), C4.4(08:52), C5.2(08:37)
27-10-2013	S12W30	320	Beta-Gamma	C1.5(01:40)
28-10-2013	S12W43	330	Beta-Gamma-Delta	
29-10-2013	S12W56	230	Beta-Gamma	M1.4(11:32)
30-10-2013	S12W71	310	Beta-Gamma	C1.3(10:36)
31-10-2013	S13W81	160	Beta	C1.8(21:33), M1.9(13:36)

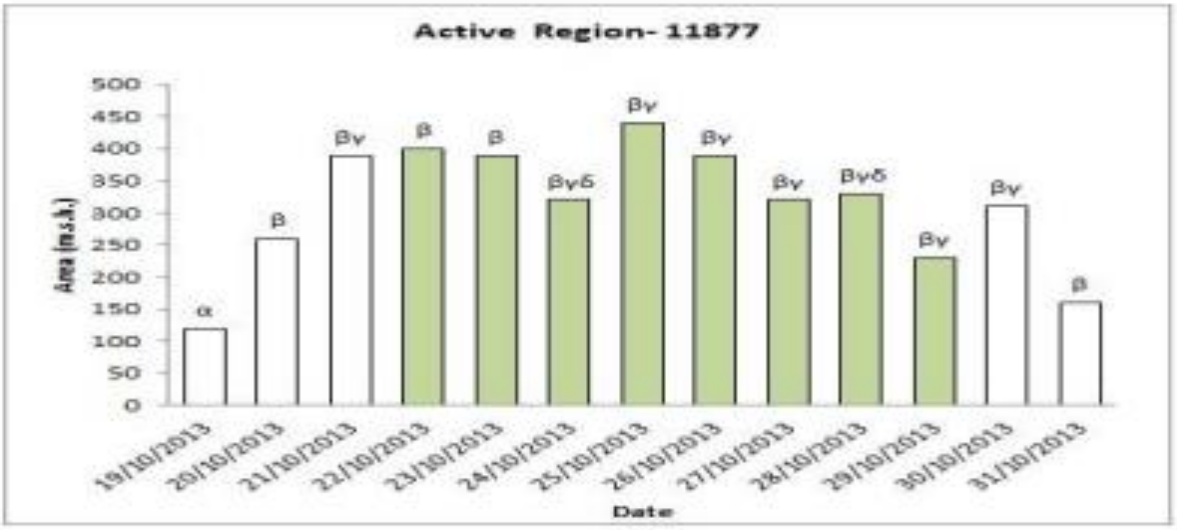

Figure 3.9: Above bar plot shows the growth of Active region NOAA 11877 observed during first reported duration 22-29 Oct 2013 in terms of area with respect to days . the shaded green bars shows the days when active region passes through ±45 degree west to east of solar disk.

Table: Show the description of Active region NOAA 11882, the first column shows date, second column indicate the location of region, third column shows area of active region, fourth

column shows the magnetic configuration type and last column indicate the flare event occurred from particular active region on particular date.

Active Region- 11882				
	Location	**Area**	**Magnetic type**	**Flare events**
25-10-2013	S08E73	100	Beta	M1.9(20:54), M2.3(19:05), M1.3(17:02), X2.1(14:51), C7.9(14:31), M1.0(09:43), X1.7(07:53), M2.9(02:48)
26-10-2013	S08E59	280	Beta-Gamma-Delta	M1.0(19:49), C2.1(18:34), C6.5(17:28), C8.8(17:06), C8.8(17:04), M1.8(10:48), M1.5(09:17), M2.3(05:59), C4.0(03:38), C2.3(03:03), C1.9(00:51)
27-10-2013	S08E47	300	Beta-Gamma-Delta	
28-10-2013	S08E34	390	Beta-Gamma-Delta	M4.4(15:07) , M2.7(14:46)

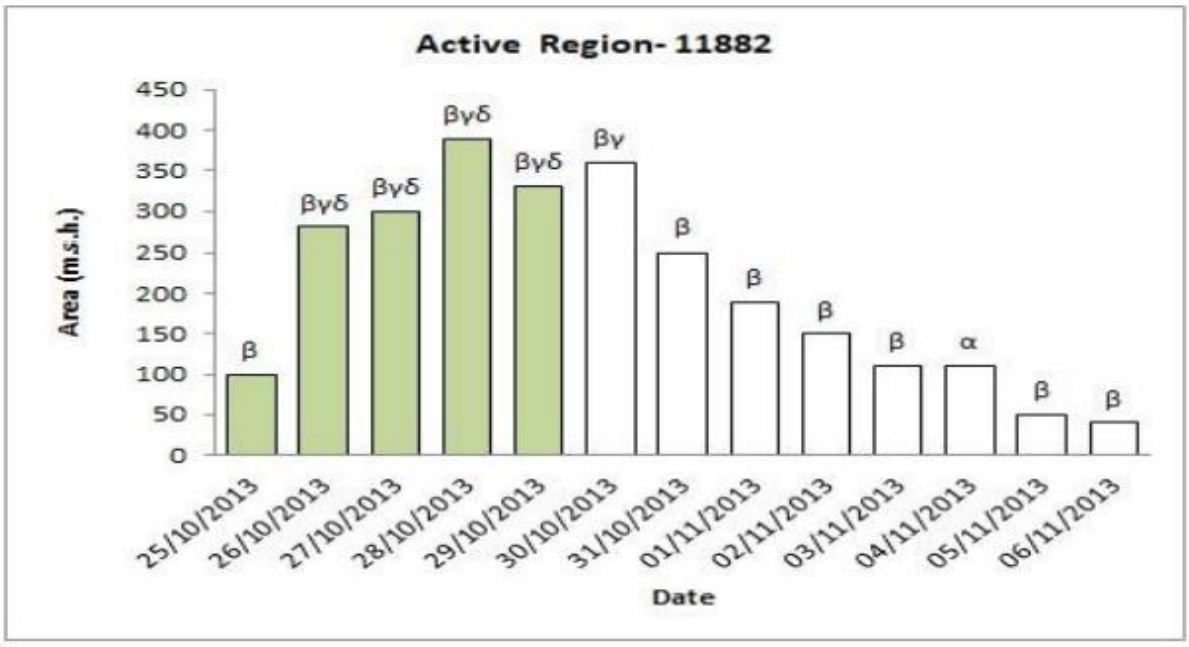

Figure 3.10: Above bar plot shows the growth of Active regions NOAA 11882 observed during first reported duration 22-29 Oct 2013 in terms of area with respect to days. The shaded green bars shows the days when active region passes through ±45 degree west to east of solar disk.

Table: Show the description of Active region NOAA 11884, the first column shows date, second column indicate the location of region, third column shows area of active region, fourth

column shows the magnetic configuration type and last column indicate the flare event occurred from particular active region on particular date.

Active Region- 11884				
	Location	**Area**	**Magnetic Type**	**Flare events**
27/10/2013	S09E78	50	Alpha	M3.5(12:36)
28/10/2013	S13E68	110	Beta-Gamma-Delta	
29/10/2013	S14E53	130	Beta-Gamma-Delta	
30/10/2013	S13E38	340	Beta-Gamma-Delta	
31/10/2013	S11E24	460	Beta-Gamma-Delta	C1.0(06:45)
11-01-2013	S12E12	370	Beta-Gamma-Delta	M6.3(19:46), C1.1(18:37), C1.8(15:17), C3.5(10:04), C1.1(09:51), C1.5(07:23)
11-02-2013	S13W01	370	Beta-Gamma	C1.7(18:08), C1.1(15:22), C4.3(12:54), C1.4(10:35)
11-03-2013	S12W13	250	Beta-Gamma-Delta	M4.9(05:16)
11-04-2013	S12W27	240	Beta-Gamma	C3.2(05:36)
11-05-2013	S12W38	110	Beta-Gamma	C2.3(16:55)
11-06-2013	S12W49	70	Beta	
11-07-2013	S12W62	50	Beta	
11-08-2013	S12W76	20	Alpha	

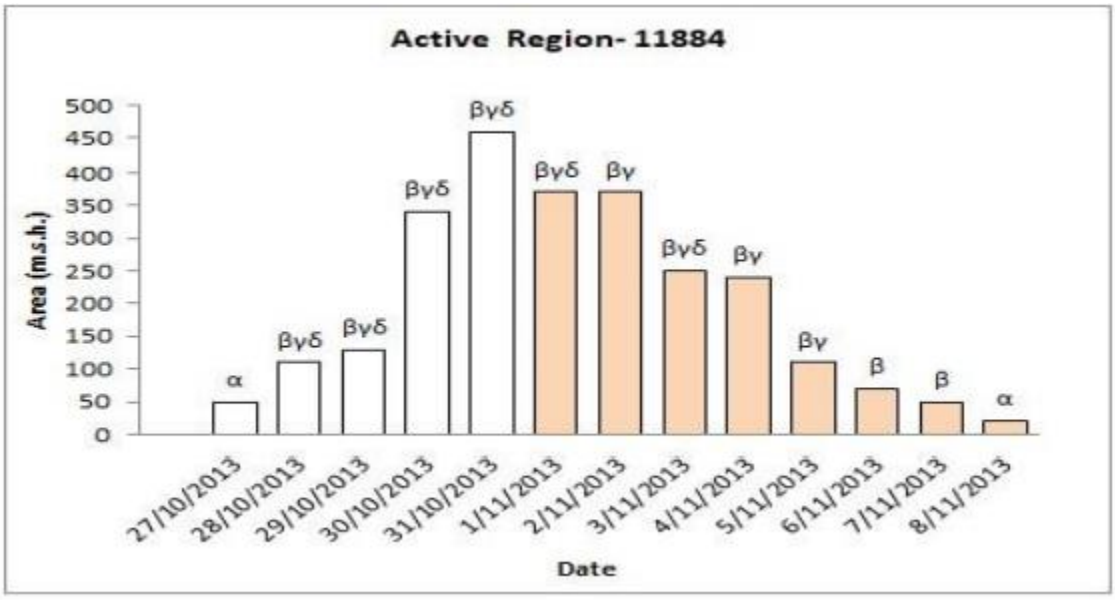

Figure 3.11: Above bar plot shows the growth of Active region (NOAA 11884) observed during first reported duration 01-08 Nov 2013 in terms of area with respect to days . The shaded pink bars shows the days when active region passes through ±45 degree west to east of solar disk.

Research Paper

Vol.11, Iss.9, Dec 2022

Table: Show the description of Active region NOAA 12192, the first column shows date, second column indicate the location of region, third column shows area of active region, fourth column shows the magnetic configuration type and last column indicate the flare event occurred from particular active region on particular date.

e-ISSN 2320 –7876 www.ijfans.org

Research Paper

Vol.11, Iss.9, Dec 2022

Active Region- 12192				
	Location	Area	Magnetic Type	Flare events
18/10/2014	S13E68	260	Beta-Gamma	C6.7(19:54), C3.8(18:59), C2.7(17:09), C2.1(17:01), C2.6(15:59), C1.7(14:22), C2.6(13:01), C3.7(06:43), C5.0(00:53)
19/10/2014	S13E56	1240	Beta-Gamma	C2.1(20:24), C4.7(17:30), C3.9(15:50), C5.8(12:08), C4.2(11:05), X1.1(04:17), C5.7(01:17)
20/10/2014	S13E43	1560	Beta-Gamma-Delta	M1.2(22:43), M1.7(19:53), M4.5(16:00), C8.6(14:58), C3.1(14:40), C2.8(11:19), M3.9(09:00), C9.0(05:37), C5.4(03:32), C3.2(02:25), C2.5(00:49)
21/10/2014	S13E30	2180	Beta-Gamma-Delta	
22/10/2014	S14E19	2410	Beta-Gamma-Delta	
23/10/2014	S12E06	2700	Beta-Gamma-Delta	X1.6(14:02), C3.2(12:00), C4.6(09:06), M2.7(05:11), M8.7(01:16)
24/10/2014	S14W06	2740	Beta-Gamma-Delta	C5.9(17:46), C4.6(15:20), M1.1(09:44), C3.7(04:19)
25/10/2014	S12W21	2510	Beta-Gamma-Delta	C5.1(14:31), C3.6(09:58)
26/10/2014	S12W34	2570	Beta-Gamma-Delta	C9.7(15:44), C5.1(15:00), C3.2(12:13), C4.6(09:44), C9.2(07:36), C9.5(06:54), C4.4(04:06)
27/10/2014	S12W46	2750	Beta-Gamma-Delta	M1.9(18:43), M4.2(18:07), C7.8(17:55), M1.0(17:08), C3.5(15:52), C5.2(15:11), C9.2(13:04), X2.0(10:04), C9.5(06:13), C4.0(05:45), C2.8(05:09), C3.1(01:08)
28/10/2014	S12W59	2380	Beta-Gamma-Delta	X2.0(14:12), C9.6(07:11), C9.6(06:56), C4.9(05:21), C3.4(05:01), M1.3(03:35), M1.0(01:44), M7.1(00:06), M1.6(13:54), C5.3(11:02), C4.2(06:06), M3.4(02:15)
29/10/2014	S13W71	2680	Beta-Gamma-Delta	C6.8(19:31), M1.3(18:47), M1.0(16:06), M1.4(14:24), C5.5(13:55), M1.2(09:54), M1.0(06:03), C8.4(03:29), C3.3(03:10)

e-ISSN 2320 –7876 www.ijfans.org

Research Paper

Vol.11, Iss.9, Dec 2022

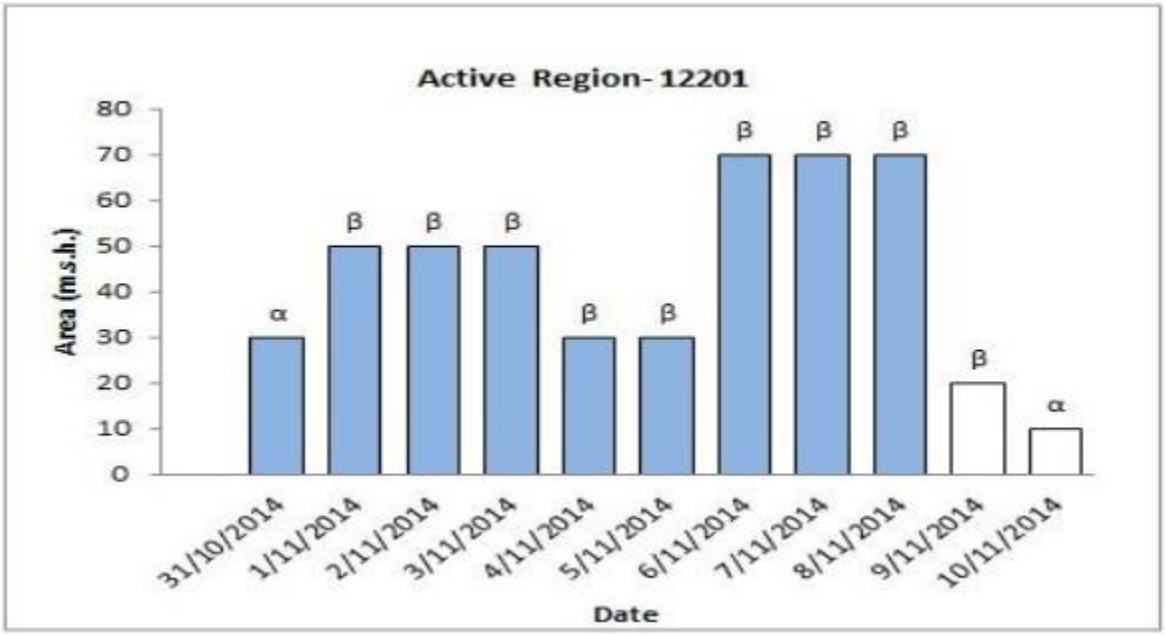

Figure 3.12: Above bar plot shows the growth of Active region (NOAA 12201) observed during third reported duration 25Oct-08Nov 2014 in terms of area with respect to days . The shaded green bars shows the days when active region passes through ±45 degree west to east from centre of solar disk.

Table: Show the description of Active region NOAA 12201, the first column shows date, second column indicate the location of region, third column shows area of active region, fourth column shows the magnetic configuration type and last column indicate the flare event occurred from particular active region on particular date.

Active Region- 12201				
	Location	Area	Magnetic type	Flare events
31/10/2014	S05E65	30	Alpha	C2.0(09:19), C2.3(08:21)
11-01-2014	S05E51	50	Beta	C2.3(18:14), C7.2(16:37), C2.6(13:42), C4.1(10:20)
11-02-2014	S05E37	50	Beta	C3.5(16:58)
11-03-2014	S05E23	50	Beta	C1.3(18:14), C1.4(04:50), C4.2(03:47)
11-04-2014	S05E10	30	Beta	
11-05-2014	S05W06	30	Beta	
11-06-2014	S05W19	70	Beta	
11-07-2014	S04W33	70	Beta	
11-08-2014	S04W48	70	Beta	
11-09-2014	S05W62	20	Beta	
11-10-2014	S05W76	10	Alpha	

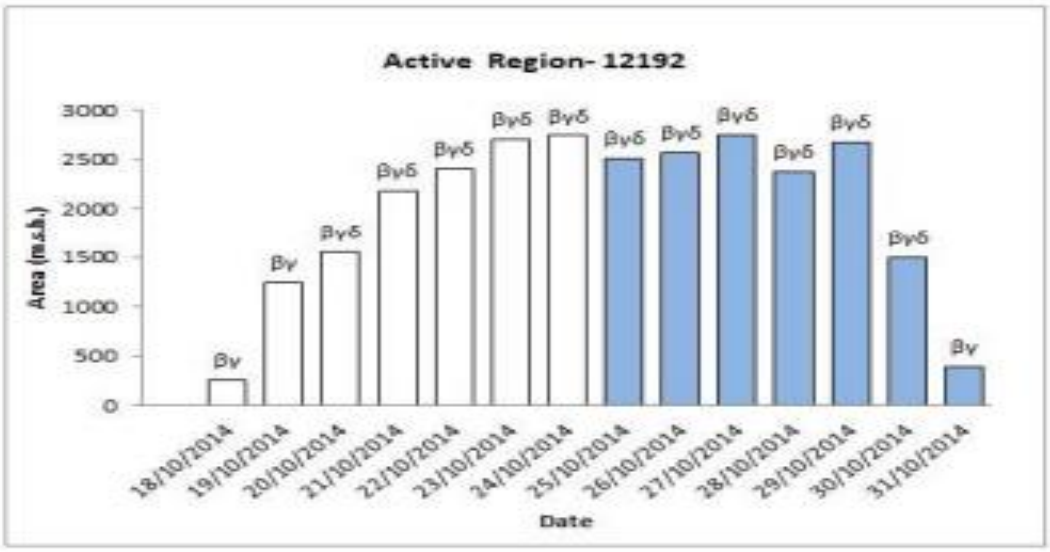

Figure 3.13: Above bar plot shows the growth of Active region (NOAA 12192) observed during third reported duration 25Oct-08Nov 2014 in terms of area with respect to days. The shaded blue bars shows the days when active region passes through ±45 degree west to east from centre of solar disk.

e-ISSN 2320 –7876 www.ijfans.org

Research Paper

Vol.11, Iss.9, Dec 2022

In this section of result we plot the GOES X-ray profile for solar flares and examine the relation between flare and CME. Figure are there GOES X-ray profile for active periods (1) 22-29 Oct 2013, (2) 01-08 Nov 2013, (3) 25Oct-08Nov 2014, (4) 07-15 March 2015 and (5) 02-10 Sep 2017 respectively. The circled peak on the plots are indication .the major X-class flare observed that particular duration. From the GOES we get flux of solar flare in two wavelength bands first 1-8Å and 0.5-4 Å. Further we have analysed the flare characteristics with CMEs. We have find out the linear relationship between flare rise time and CME speed; decay time of flare verses speed of CMEs and total duration of flare versus CMEs speed. From the figure we can see that for first active period (22-29 Oct 2013) there is no good relation between CME speed and rise time; decay time and total duration of flare. This may be due to the mixed classes of flare observed in that duration. From Table we can see the observed flare in first duration and their association with CMEs, the CME associated flares are in C-class, M-class and X-class. We got less correlation in second duration (01-08 Nov 2013) due to the similar reason as first active period. While we obtained the good correlation between CME speed and flare's features in all the three cases (rise time, decay time and total duration).

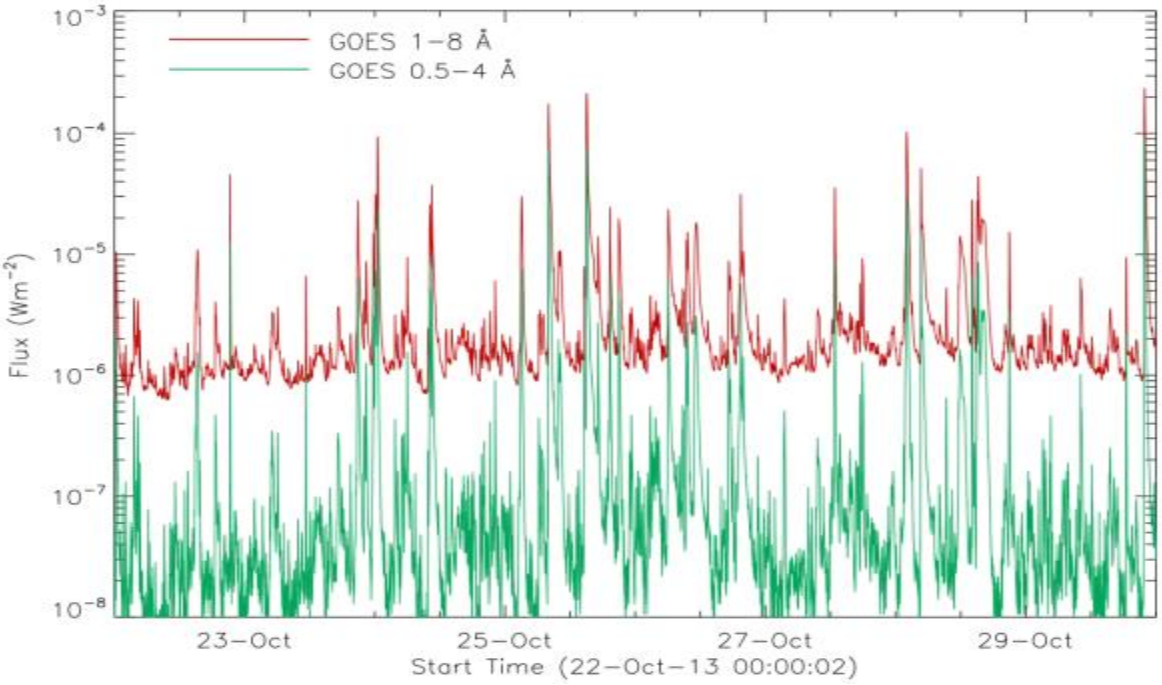

Research Paper

Vol.11, Iss.9, Dec 2022

Figure 3.15: Shows the GOES X-ray profile for solar flare observed during first reported active period 22-29 Oct 2013. The Marked peak indicate the X-class flares during the period.

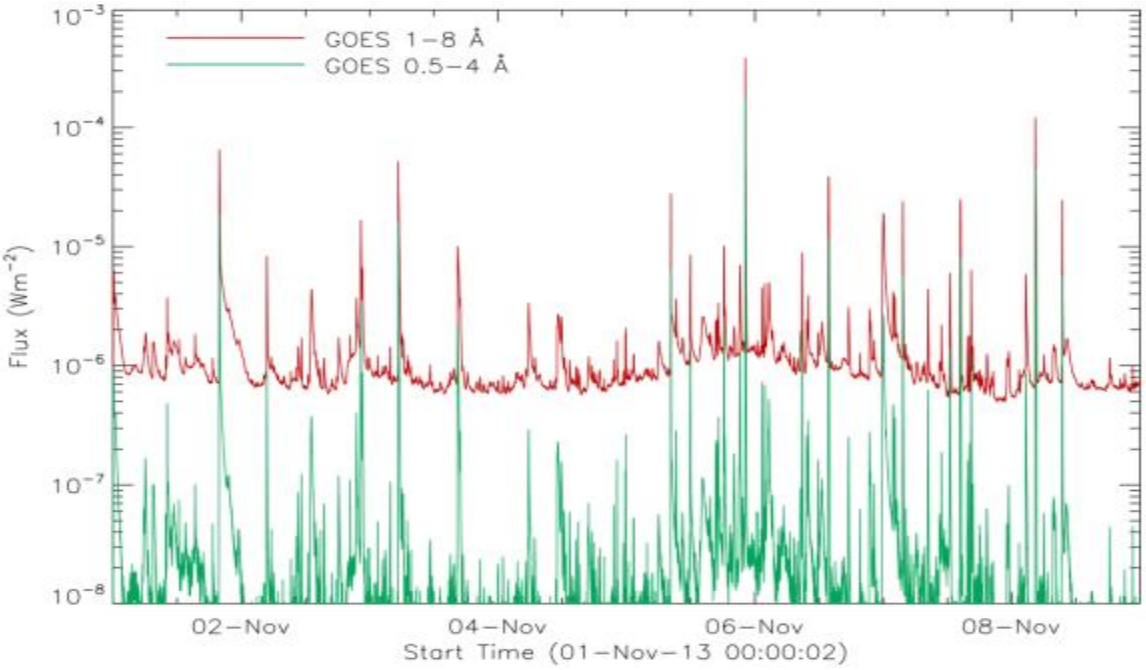

Figure 3.16: Shows the GOES X-ray profile for solar flare observed during first reported active period 25Oct-17Nov 2014. The Marked peak indicate the X-class flares during the period.

CONCLSUION

The nature and scales of magnitude of solar flares are fairly well understood scientifically. And yet, every solar flare has some unique features that essentially need to be explored. While studying solar flares during the present work we had a specific planning: We chose two extremes of solar flares, viz., the large solar flare such as X-class and a small scale activity. The same is suggested to be undertaken to understand the correlation between the small scale activity and a large scale activity on large number of occasions. And a rigorous study over a large number of solar activities would enable us to understand emissive phenomena in a better way.

Another hind side of the eruption of solar flares is the effect of solar flares on the spaceweather. We ought to understand the effect of solar flares on the space weather as precisely as possible as the space weather is vital for the economic activity and the survival of life on the Earth.

Research Paper

Vol.11, Iss.9, Dec 2022

The research presented in this thesis gives us an excellent insight into photospheric and coronal magnetic field evolution of in the flaring regions. For the first time, vector magnetic field changes have been observed merely hours before small magnitude flares. Also, changes in the vector magnetic field observed after the flare occurrence have confirmed current models of field configuration variations due to flares. Any future research expanding upon the first detections presented here will be extremely beneficial in furthering our understanding of the magnetic nature of active regions and solar are processes.

Small scale activity plays important role in converting magnetic energy into thermal energy. It is important to investigate energy budget of such activity to understand energy transfer to upper atmosphere. We need to do more analysis of flaring and non-flaring active region study to understand if such activity has any role in magnetic field formation that can trigger flares.

The flare activity hitherto studied, at large and small scale scenario, needs to be compared with simulations, particularly, recent simulations extended from upper atmosphere (Rempel 2017). We also need to study from these simulations: How magnetic field variations in photosphere can trigger flare and small scale activity above active region?

Chromospheric Magnetic Field observations have been used throughout this thesis in order to find regions of interest for this study (where are peak brightening occurs). A deeper investigation of chromospheric observations could be an interesting exercise for future research. We feel that Chromospheric vector magneto-grams rather than photospheric vector magnetograms would be more accurate inputs to 3D extrapolation procedures, since preprocessing basically emulates chromospheric conditions in order to reach a state closer to a force-free state. Although, data of chromospheric magnetic field is presently not widely available, but, with the launch of the Solar-C spacecraft in 2018 will provide these measurements at much higher spatial resolution and polarimetric accuracy than currently available from HINODE (Solar-B). The new instruments on DIKIST will record photospheric and chromospheric vector magnetic field data at much better spatial resolution (compared to 0.32" for SOT-SP) and better polarimetric accuracy.

Though, we studied various parameters related to flaring active region and small scale activity other parameters remain left out of these studies. For example, one pertinent open question remains: How does helicity evolve in the regions of these studies? Better knowledge of the helicity changes with time before and after a flare are the events that may help us to quantify various

aspects of the magnetic field structure (see Berger, 1999). Particularly, this would be useful for the better understang of 25th February, 2014 event, as it would complement the 3D geometry and energy values observed. Also, a discovery about conservation of helicity in the AR studied would help place the partial Taylor relaxation observed into a wider context.

Though, vector magnetic field variations during small scale activity are well studied, we need to study vector magnetic field variation before, during and after flare with more statistics. The great advantage of HMI analysis is that it provides vector magnetic field data at better temporal resolution. We need to use HMI data with AIA, HINODE and IRIS for a better understanding of vector magnetic field variations.

REFERENCES

1. Aschwanden, M. J. (2004), _Physics of the Solar Corona: An Introduction‘, PRAXIS, Chichester, UK, Springer, Berlin, 2004.

2. Aschwanden, M. J. (2007), _RHESSI Timing Studies: Multi-Thermal Delays‘, The Astrophysical Journal, 661, pp. 1242-1252.

3. Aschwanden, M. J. (2010), _Self Organizing Criticality in Astrophysics‘, Solar and Astrophysic Journal, 722, pp. 122-130; arXiv:1012.1586 [astro-ph.SR].

4. Assembly (AIA) on the Solar Dynamics Observatory (SDO) (2010), Solar Physics, 275 (1). pp. 217-240.

5. Battaglia, M., Fletcher, L., and Benz, A. O. (2009), Astronomy & Astrophysics, 498 (3), pp. 891- 900.

6. Bharti, L., Hirzberger, J., Solanki, S.K. (2013), Fine structures in the atmosphere above a sunspot umbra. Astronomy & Astrophysics. 552, L1-L5.

7. Bharti, L., Solanki, S.K., Hirzberger, J. (2010), Evidence for Convection in Sunspot 79 Penumbrae, The Astrophysical Journal Letters, 722, L194-L198.

8. Bharti, L., Solanki, S.K., Hirzberger, J. (2017), Lambda-shaped jets from a penumbral intrusion into a sunspot umbra: a possibility for magnetic reconnection. Astronomy & Astrophysics. 597, A127 (1-7).

9. Brandenburg, A. and Subramanian, K. (2005), _Astrophysical Magnetic Fields and Nonlinear Dynamo Theory‘, Physics Reports, 617, pp. 1-209.

10. Brown, J. C. (1971), _The deduction of energy spectra of non-thermal electrons in flares in X-ray bursts‘, Solar Physics, 18, pp. 489-502.

11. Canfield, R. C., Hudson, H. S., Leka, K. D., Mickey, D. L., Metcalf, T. R., Wuelser, J., Acton,L. W., Strong, K. T., Kosugi, T., Sakao, T., Tsuneta, S., Culhane, J. L., Phillips, A., and Fludra , A. (1992), Publications of Astronomical Society of Japan, 44, L111-115.

12. Castelli, J. P. and Richards, D., W. (1971), Journal of Geophysical Research, 76, p. 8409.

13. Chang, L., Lee, J., Dale, E., Gary, and Wang, H. (2007), The ribbon-like hard x-ray emission in a sigmoidal solar active region, The Astrophysical Journal, 658 (2) pp. L127- L130

14. Cowling, T., G., Solar Electrodynamics, Electromagnetic Phenomena in Cosmic Physics, Proceedings from IAU Symposium No. 6. (Edited by B. Lehnert, International Astronomical Union, Symposium No. 6 (2000) Cambridge University Press, p.105.)

15. Culhane, J. L. (2007), —HINODE EUV Study of Jets in the Sun‘s South Polar Corona‘, Publications of the Astronomical Society of Japan, 59, pp. S451-S457.

16. Culhane, L.K. Harra, A.M. James, K. Al-Janabi, L.J. Bradley, R.A. Chaudry, K. Rees, J.A. Tandy, P. Thomas, M.C.R. Whillock, B. Winter, G.A. Doschek, C.M. Korendyke, C.M. Brown, S. Myers, J. Mariska, J. Seely, J. Lang, B.J. Kent, B.M. Shaughnessy, P.R. Young, G.M. Simnett, C.M. Castelli, S. Mahmoud, H. Mapson-Menard, B.J. Probyn, R.J. Thomas, J. Davila, K. Dere, D. Windt, J. Shea, R. Hagood, R. Moye, H. Hara, T. Watanabe, K. Matsuzaki, T. Kosugi, V. Hansteen, O. Wikstol, (2007), _UV Imaging Spectrometer for Solar-B‘, Solar Physics, 243, pp. 19-21; doi:10.1007/s01007-007-0293-1

17. Culhane, J. L. and Jordan, C. (Eds. 1991), —The Physics of Solar Flares‖, Proceedings of RoyalSociety of London. (See reference therein) Culhane, J. L., Harra, L. K., James, A. M., Al-Janabi, K., Bradley, L. J., and Chaudry, R. A. (2007), The EUV imaging spectometer for HINODE', Physics. 243 (1), pp.19-61.

18. Dennis, B. R., Zarro, D. M. (1993), The Neupert Effect: What Can it Tell us about the 81 Impulsive and Gradual Phases of solar Flares? Solar Physics, 146, pp. 177-190.

19. Dryer, M., Andrews, M., D., Michels, D., J., Paswaters, S., E., and Tappin, S., J. (1998), _The Solar Minimum Active Region 7978, Its 2.6X/1B Flare, CME and Interplanetary Shock Propagation on 9 July 1996‘, Solar Physics, 181, pp. 159-183.

Research Paper

Vol.11, Iss.9, Dec 2022

20. Felipe, T., Collados, M., Khomenko, E., Rajaguru, S.P., Franz, M., Kuckein, C., Asensio Ramos, A.: (2017), Signatures of the impact of flare ejected plasma on the photosphere of a sunspot light-bridge. arXiv: 1708.06133.

21. Fisher, G., H., Welsch, B., T., Abbett, W., P. and Bercik, D., J. (2010), _Estimating electric fields from vector magnetogram sequences', The Astrophysical Journal, 715, pp. 242-259.

22. Fisher, G., H., Welsch, B., T. and Abbett, W., P. (2012), _Can we determine electric fields and Poynting fluxes', Solar Physics, 277, pp. 153-160.

23. Fisher, G., H., Abbett, W., Bercik, P., D., J., Kazachenko, M., D., Lynch, B., J., Welsch, B., T., Hoeksema, J., Hayashi, T., K., Liu, Y., Norton, A., A., Sainz, A. and Dalda, X., De Rosa, M., L. and Cheung, M., C., M. (2015), _The Coronal Global Evolutionary Model: Using HMI Vector Magnetogram and Doppler Data to Model the Buildup of Free Magnetic Energy in the Solar Corona', Space Weather 13 (6), pp. 369-373.

24. Hudson, H. S. (1991), Differential Emission- Measure Variations and the —Neupert Effect‖, Bulletin of American Astronomical Society, 23, p. 1064.

25. Ichimoto, K., Suematsu, Y., Tsuneta, S., Katsukawa, Y., Shimizu, T., Shine, R.A., Tarbell, T.D., Title, A.M., Lites, B.W., Kubo, M., Nagata, S. (2007), Twisting Motions of Sunspot Penumbral Filaments. Science, 318, pp. 1597-1599.